Journal of Biomechanics 97 (2019) 109356

Contents lists available at ScienceDirect

Journal of Biomechanics

journal homepage: www.elsevier.com/locate/jbiomech
www.JBiomech.com

Concurrent validity of a wearable IMU for objective assessments of functional movement quality and control of the lumbar spine

Kristen H.E. Beange [a,c], Adrian D.C. Chan [a,b,c], Shawn M. Beaudette [b], Ryan B. Graham [b,c,*]

[a] Department of Systems and Computer Engineering, Faculty of Engineering and Design, Carleton University, 1125 Colonel By Drive, Ottawa, Ontario K1S 5B6, Canada
[b] School of Human Kinetics, Faculty of Health Sciences, University of Ottawa, 200 Lees Avenue, Ottawa, Ontario K1N 6N5, Canada
[c] Ottawa-Carleton Institute for Biomedical Engineering, Ottawa, Ontario, Canada

ARTICLE INFO

Article history:
Accepted 18 September 2019

Keywords:
Inertial measurement units
Low back pain
Movement quality
Continuous relative phase
Local dynamic stability

ABSTRACT

Inertial measurement units (IMUs) are being recognized in clinical and rehabilitation settings for their ability to assess movement-related disorders of the spine for better guidance of treatment-planning and tracking of recovery. This study evaluated the Mbientlab MetaMotionR IMUs, relative to Vicon motion capture equipment in measuring local dynamic stability of the spine (quantified using maximum finite-time Lyapunov exponent; λ_{max}), lumbopelvic coordination (quantified using mean absolute relative phase; MARP), and intersegmental motor variability (quantified using deviation phase; DP) of lumbopelvic segments in 10 participants during 35 cycles of repetitive spine flexion–extension (FE). Intraclass correlations were strong between systems when using both the FE angle time-series and the sum of squares (SS) time-series to measure local dynamic stability ($0.807 \leq ICC_{2,1}^{\lambda max,FE} \leq 0.919$; $0.738 \leq ICC_{2,1}^{\lambda max,SS} \leq 0.868$), sagittal-plane lumbopelvic coordination ($0.961 \leq ICC_{2,1}^{MARP} \leq 0.963$), and sagittal-plane lumbopelvic variability ($0.961 \leq ICC_{2,1}^{DP} \leq 0.963$). It was concluded that the MetaMotionR IMUs can be reliably used for measuring features associated with spine movement quality and motor control during a repetitive FE task. Future work will assess the reliability of sensor placement, performance during multi-directional movements, and ability to discern clinical and healthy populations based on assessment of movement quality and control.

1. Introduction

Low back pain (LBP) is the leading cause of disability worldwide, affecting over 500 million people annually across the globe (Vos et al., 2016). The majority of these cases (up to 90%) are classified as 'non-specific' (Maher et al., 2017; Waddell, 2004), meaning that the pain cannot be attributed to any specific injury or pathology (Dillingham, 1995). Further, the majority of current treatment strategies address signs and symptoms (i.e., short-term treatment) while overlooking the specific dysfunction underlying the low back disorder (i.e., long-term treatment and solution; Azevedo et al., 2018; O'Sullivan, 2005). As a result, low back disorders that may otherwise be treatable persist into chronic and/or recurrent cases (Hoy et al., 2010).

It is understood that the LBP patient-population presents with highly heterogeneous motor control phenotypes that are indicative of dysfunction and pathological pain development (Hemming et al., 2018; O'Sullivan, 2005; van Dieën et al., 2018b; Wattananon et al., 2017). Through investigating this range of motor control behaviour, it is believed that specific subgroups of dysfunction may be distinguished, which can help clinicians objectively administer a more effective, personalized standard of care (Fritz et al., 2007; van Dieën et al., 2018b, 2018c). Despite this shift toward assessment of spine movement quality and control to stratify 'models of care' for LBP patients, there is poor inter- and intra-rater reliability in terms of visual appraisal of these features when performed by healthcare professionals (Biely et al., 2014; Hicks et al., 2003; Stanton et al., 2011). Additionally, visual appraisal of spine movement restricts assessments to metrics that are detectable by the human eye (e.g., range of motion, judder). As such, objective assessments of movement features are an important future direction for overall LBP management (Spinelli et al., 2015).

Local dynamic stability (LDS) and continuous relative phase (CRP) are two common features that have been extensively studied in the investigation of dynamic spine motor control (Graham et al., 2014; Silfies et al., 2009; Spinelli et al., 2015). These metrics estimate the interactions of the time-varying biological systems required to achieve control of dynamic spine movement. LDS

* Corresponding author at: University of Ottawa, Faculty of Health Sciences, Ottawa, ON K1N 6N5, Canada.
E-mail address: rgraham@uottawa.ca (R.B. Graham).

https://doi.org/10.1016/j.jbiomech.2019.109356
0021-9290/

quantifies the level of chaos within a system; with respect to spine movement, it characterizes one's ability to achieve and maintain movement stability during dynamic tasks in the presence of internal (i.e., local) perturbations inherent in the neuromuscular control system. LDS is quantified through the estimation of the maximum finite-time Lyapunov exponent (λ_{max}), which is calculated by locating nearest neighbouring trajectories in a reconstructed state space, and then determining the exponential growth (i.e., divergent/unstable behaviour, represented by a positive λ_{max} value) or decay (i.e., convergent/stable behaviour, represented by a negative λ_{max} value) of neighbouring trajectories through time (Rosenstein et al., 1993). λ_{max} always yields a positive value (as the spine is inherently unstable), and, while there is no optimal value for λ_{max}, it is believed that the general population follows a Gaussian distribution, where higher positive values of λ_{max} are indicative of "loose" control of the spine (i.e., proprioceptive deficits), and lower positive values of λ_{max} are indicative of "tight" control of the spine (i.e., muscle guarding and kinesiophobia) – dysfunctions benefiting from vastly different treatments (Hodges et al., 2013; van Dieën et al., 2018a, 2018b).

CRP analyses reveal elements of sequential movement patterns, and are well-suited to portray spatiotemporal coordination and variability of human movement subsystems (e.g., thoracic and lumbar spine regions) over time. CRP is determined by calculating the relative phase angle (PA) from a parametric phase plot (normalized angular displacement vs. normalized angular velocity) of adjacent segments (Lamb and Stöckl, 2014). CRP waveforms can be interpreted visually, or by calculating the coordination (i.e., mean absolute relative phase (MARP); by taking the average of the 'mean CRP curve') and variability (i.e., deviation phase (DP); by taking the average of the 'mean standard deviation (SD) curve'). Functionally, low MARP indicates a more in-phase coordination between segments, and high MARP indicates an out-of-phase coordination (Stergiou et al., 2001). Moreover, low DP indicates less variability between cycles, and high DP indicates more variability between cycles (Stergiou et al., 2001). Both LDS and CRP have been identified in their ability to discern normal and abnormal spine movement behaviour (Asgari et al., 2017; Beaudette et al., 2019), as well as healthy versus LBP populations (Asgari et al., 2015, 2017; Bauer et al., 2015b).

These measures are computed based on spine movement data and are extensively studied in laboratory settings using conventional motion capture systems (e.g., optical motion capture). While these systems provide accurate and reliable data, the cost and complexity are prohibitive for common clinical practice. Inertial measurement units (IMUs) are being recognized as a portable and cost-worthy alternative to conventional motion capture systems, and have the potential to be introduced into clinical settings as an objective tool to assess functional control of the spine (Ashouri et al., 2017). The introduction of IMU-based assessments into routine clinical practice can both: (a) provide healthcare professionals with the ability to objectively score and assess features that are currently visually assessed (e.g., lumbo-pelvic rhythm, judder; Wattananon et al., 2017), and (b) expand upon current features assessed in clinics by including features that are visually undetectable (e.g., LDS, MARP, and DP). However, due to both insufficient evidence of sensor validity and the lack of understanding surrounding laboratory-based features and their respective clinical applications, IMU-based assessments have not yet been integrated into routine clinical practice (Bauer et al., 2015a; Bolink et al., 2016; Cuesta-Vargas et al., 2010; Whelan et al., 2016).

Several researchers have shown success in investigating elements of gross dynamic control of the spine using objective and wearable-based evaluations in experimental settings (Bauer et al., 2015a; Beange et al., 2019; Kim and Nussbaum, 2013; Laird et al., 2016); however, it is not yet clear if these types of assessments are clinically suitable. Therefore, the purpose of this study was to validate IMUs for the assessment of functional movement quality metrics of the lumbar spine relative to gold-standard methods of motion analysis. More specifically, this study is designed to assess the accuracy and reliability of the MetaMotionR IMUs (~$80USD; Mbientlab Inc., San Francisco, USA) compared to a 10-camera passive optical motion capture system (Vicon Vantage V5 cameras; 5 megapixels; Vicon Motion Systems Ltd., Oxford, UK) in capturing features associated with spine movement quality and control.

2. Methods

2.1. Participants

Ten healthy adults (4F/6M) were recruited to participate in this study (Table 1). All participants provided informed consent prior to data collection and all procedures were approved by the institutional Research Ethics Board. Participants with a history of LBP or those having experienced any significant musculoskeletal injury $\leq$6 months prior to the testing day were excluded.

2.2. Instrumentation

MetaMotionR IMUs were adhered to two rigid plates with four passive reflective markers in each of the four corners (Fig. 1) to ensure each system is tracking the same movements. Rigid plates were firmly attached to the participant superficial to the T_{10}-T_{12} spinous processes, and over the sacrum using a palpation technique, while the participant was assuming a standing neutral posture (Fig. 1) so that the IMUs lined up with T_{11} and S_2 vertebral bodies. Fused Euler IMU data (depicting the absolute roll, pitch and yaw orientation of each sensor) were collected via Bluetooth Low Energy by means of the Mbientlab Inc. MetaBase mobile application. The sensor fusion algorithm obtained from the BSXlite Fusion Library (Bosch Sensortec GmbH, Reutlingen, Germany) includes offset calibrations of magnetometer and gyroscope sensors to account for influences from magnetic distortion and gyroscopic drift, respectively, calibration of the accelerometer and compass orientation (i.e., tilt compensation), Kalman filter, and limits to inter-frame timing deviation (Bosch Sensortec, 2015). Data were collected from both systems at 100 Hz.

2.3. Movement protocol

Emulating previous protocols, participants performed 35 spine flexion–extension (FE) cycles while constrained at the hip (Granata and England, 2006; Howarth and Graham, 2015). They were instructed to touch two targets with their hands outstretched in front of them in synchrony with a metronome at 0.5 Hz (i.e., 2 s between targets/4 s per cycle); one target was placed at shoulder height directly in front of the participant and the other was placed 50 cm anterior to the knee (Fig. 2). One complete cycle was defined as movement from a fully flexed position, into an upright position, and back to full flexion.

Table 1
Mean participant age, height and mass characteristics. Errors (in brackets) depict standard deviations.

Demographic	Male	Female
n	6	4
Age (years)	25.3 (2.2)	22.8 (2.2)
Height (cm)	180.5 (2.3)	165.0 (10.3)
Mass (kg)	81.9 (4.0)	58.4 (3.9)

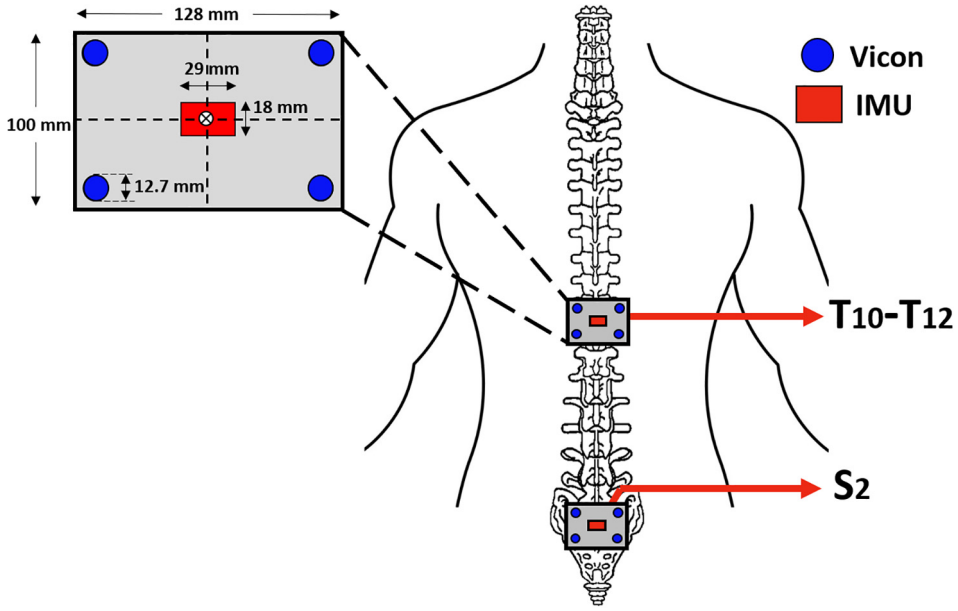

Fig. 1. Sensor setup and configuration. Inertial measurement units (IMUs; red) are adhered to a rigid plate (grey), with four passive reflective markers (blue) in each corner. Rigid plates are placed superficial to the T_{10}-T_{12} spinous processes and the sacrum (S_2). Configuration dimensions are given in an exploded view of the thoracic rigid body marker cluster/IMU setup (top left). (For interpretation of the references to colour in this figure legend, the reader is referred to the web version of this article.)

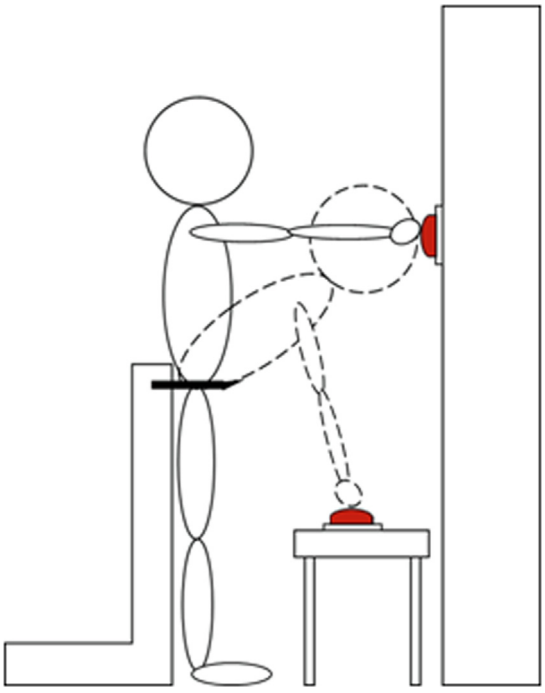

Fig. 2. Flexion-extension task. Participants begin in a fully flexed position, with arms extended below them (dashed line), then extend their back until they reach an upright position, with arms extended in front of them (solid line), and back to full flexion to complete one full cycle.

2.4. Data processing and analysis

2.4.1. Kinematic data

The first five cycles of FE were excluded from both Vicon and IMUs to ensure steady-state motion (e.g., Graham et al., 2012a; Granata and England, 2006). The remaining 30 cycles from Vicon and MetaMotionR IMUs were synchronized using the first peak value in the sagittal/FE plane angular time-series (i.e., the sixth peak in the original time-series) and low-pass filtered with a zero-phase Butterworth filter (effective 4th order with a cutoff frequency of 3 Hz) to attenuate unwanted noise (Winter, 2010). Any gyroscopic drift that was not successfully removed via on-board sensor fusion was removed by subtracting a least-squares line of best-fit from the time-series. IMU Euler data were converted to a 3×3 rotation matrix, and relative sensor motion was calculated using a sagittal-frontal-transverse rotation sequence. Similar right-handed coordinate systems were created for Vicon rigid-body marker clusters, and transformation matrices were generated to mirror the IMU relative motion estimates. Data from both systems were then converted to Euler angles for calculation of movement control metrics. Individual axes were normalized to a standing position by subtracting the signal from the mean of the first 100 frames of the original time-series prior to cutting; this was done to minimize effects of local coordinate systems misalignments between the IMUs and Vicon.

2.4.2. Local dynamic stability

LDS was quantified by implementing a method of time-delays to IMU and Vicon angular data in order to determine λ_{max} (Rosenstein et al., 1993). This process was done using both the sum of squares (SS) of the 3D relative Euler angles as well as FE data alone. The SS was calculated using Eq. (1), where θ_{FE} is the FE angle, θ_{LB} is the lateral bend angle, and θ_{AT} is the axial twist angle.

$$SS_i = \sqrt{\theta_{FE_i}^2 + \theta_{LB_i}^2 + \theta_{AT_i}^2} \quad (1)$$

To accommodate different signal lengths, each signal was time-normalized to 12,000 (30 cycles $\times$ 4 s/cycle $\times$ 100 Hz) samples (Bruijn et al., 2009a). A 6-dimensional state space for the time-series was reconstructed using a time-delay of 40 samples (i.e., 10% of the average number of samples per cycle; Graham et al., 2012a; Graham and Brown, 2012; Granata and England, 2006). The exponential rate of divergence (λ_{max}) between nearest neighbour trajectories in the reconstructed state space was determined by estimating a line of best-fit across the first 0.5 cycles of the aver-

age logarithmic divergence curve using both the SS and FE time-series (Bruijn et al., 2009a, 2009b, Graham et al., 2012a, 2012b; Fig. 3).

2.4.3. Coordination and variability

Coordination and variability were calculated using CRP curves on FE data (Fig. 4). First, segment angular velocity was calculated by taking the derivative of the thoracic and sacral IMU/marker cluster angular positions using the three-point central finite differences method (Graham et al., 2015; Lamb and Stöckl, 2014). All segment angles and velocities were then divided into individual FE cycles, as defined by successive maximum flexion angles, and interpolated to 101 data points corresponding to 0–100% of the FE cycle. Segment angular positions (θ) and velocities (ω) were phase-normalized from −1 (minimum) to +1 (maximum) as per Eq. (2) to minimize effects of signal amplitude and frequency on the calculation of the segment PA (Peters et al., 2003).

$$\theta_{i,norm} = 2 \times \frac{\theta_i - \min(\theta)}{\max(\theta) - \min(\theta)} - 1 \quad (2)$$

Phase portraits were created by plotting normalized angular positions against the normalized angular velocities (Peters et al., 2003). PAs (φ) were calculated at each time point of the FE cycle using a four-quadrant inverse tangent function, and defined as the angle from the right horizontal axis (Hamill et al., 2012; Seay et al., 2011). All PAs ranged from −180° to +180°. CRP angles were obtained by subtracting the absolute PA of the distal segment (thoracic spine) from the absolute PA of the proximal segment (sacral spine; Eq. (3)).

$$CRP_i = \left|\varphi_{i,proximal} - \varphi_{i,distal}\right| \quad (3)$$

MARP was calculated by taking the average of the mean ensemble curve (i.e., the curve representing the average PA at each percentage of the FE cycle, across all 30 cycles; Eq. (4)).

$$MARP = \sum_{i=1}^{101} \left|\varphi_{relativephase}\right|_i / 101 \quad (4)$$

DP was calculated by taking the average of the mean SD ensemble curve (i.e., the curve representing the SD at each percentage of the FE cycle, across 30 cycles; Eq. (5)).

$$DP = \sum_{i=1}^{101} SD_i / 101 \quad (5)$$

MARP and DP were calculated over three time-bands: (1) 0–100% of the cycle (representing extension-flexion), (2) 0–50% of the cycle (representing extension), and (3) 50–100% of the cycle (representing flexion). This was done to assess reliability in calculating different movement strategies (e.g., leading vs. lagging segments and degree of variability) across different periods of movement in the FE cycle.

2.5. Statistical analysis

All statistical calculations were performed in SPSS 25 (IBM Corporation, Armonk, USA). Bland-Altman plots were used to assess level of agreement between IMUs and Vicon, and intraclass correlation coefficients ($ICC_{2,1}$) were applied to determine correlation of λ_{max}, MARP, and DP. Tests for normality revealed normal distributions in most cases. In cases where data were not normally distributed, normality was achieved by computing the inverse of the data. Statistically, $ICC_{2,1}$ values above 0.7 represent strong positive agreement, with 1.0 being perfect agreement (Cohen, 1988). Values

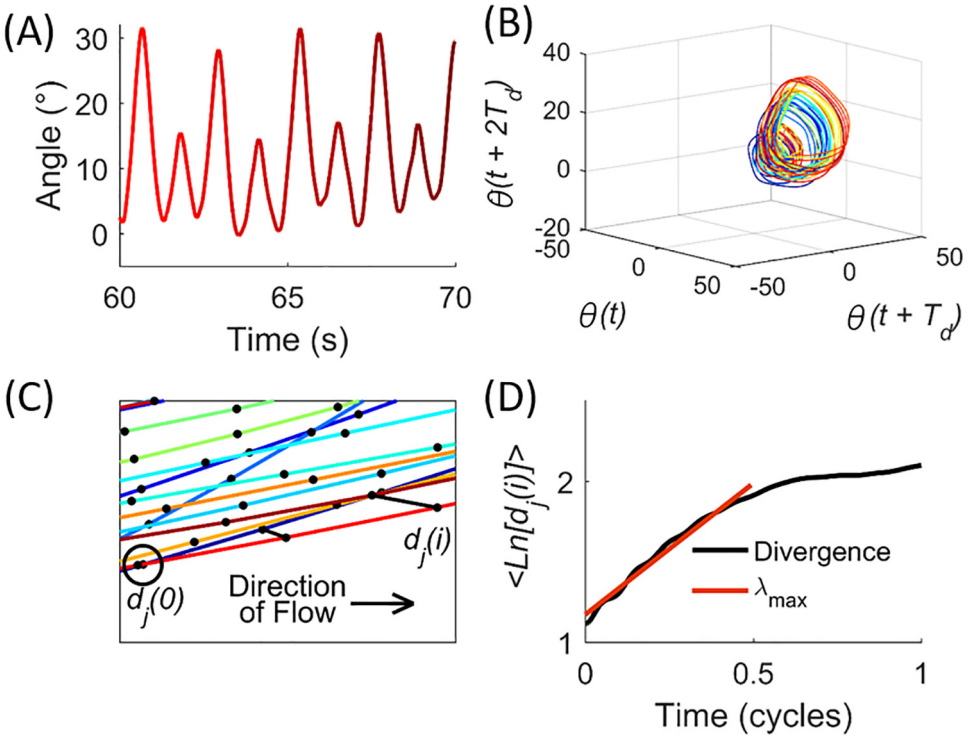

Fig. 3. Calculation of local dynamic stability. The sequencing of events is illustrated in the colour contour of the time-series; the task begins with the colour blue and transitions into red to denote the end portion of the task. (A) Zoomed in view of the flexion–extension (FE) time-series. (B) Reconstructed dynamics of the FE motion in 3-dimensional state space using a time delay of 0.4 s (note that 6 dimensions were actually used for reconstruction, but cannot be displayed visually). (C) Expanded view of a local region on the reconstructed attractor, displaying diverging FE distance (d_j) of nearest neighbour pairs after an infinitesimally small perturbation. (D) Average logarithmic rate of divergence of all nearest neighbour trajectories over one flexion cycle. Short-term maximum finite-time Lyapunov exponents (λ_{max}) were calculated using the slope of the curve from 0 to 0.5 FE cycles.

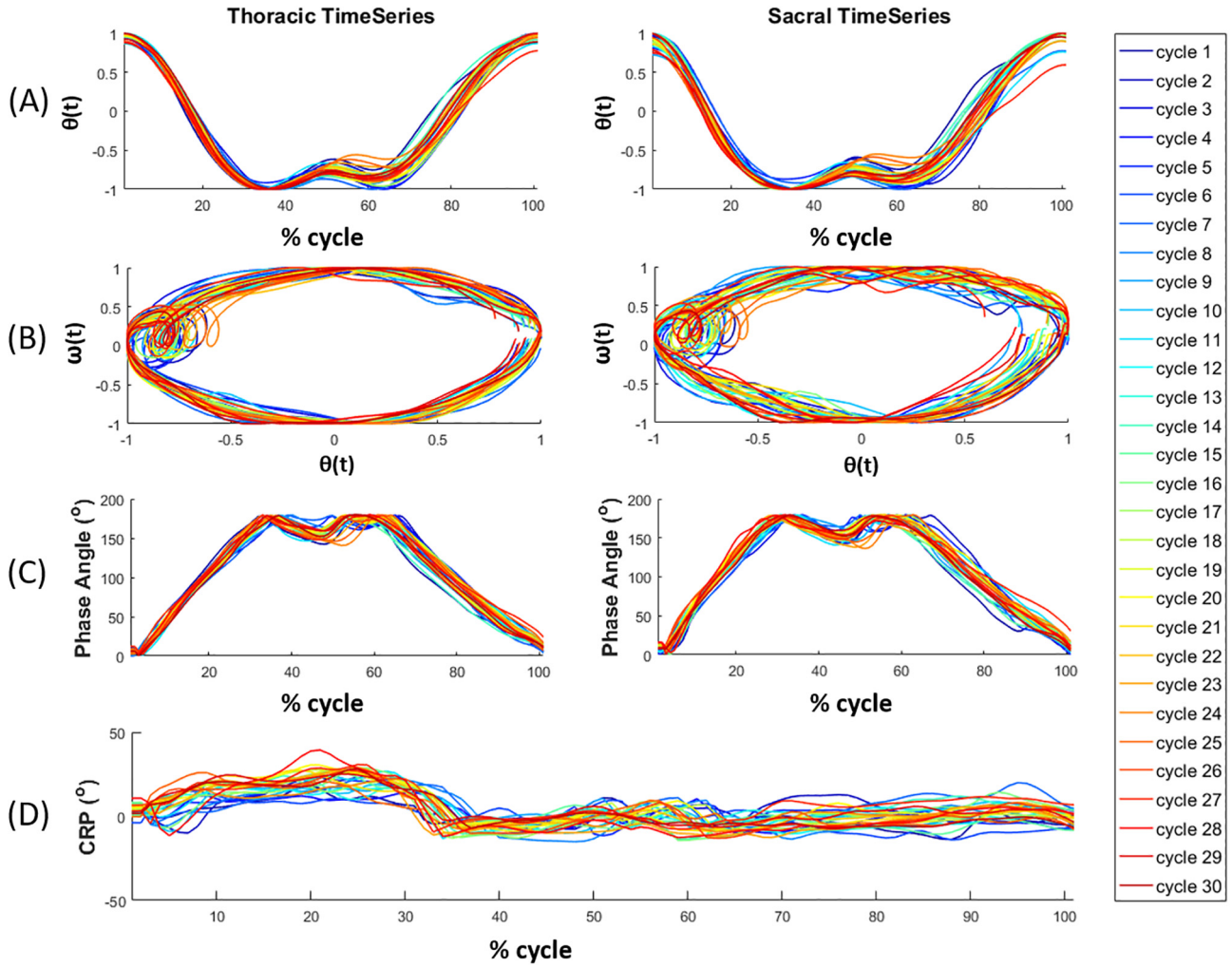

Fig. 4. Calculation of continuous relative phase (CRP) angle. The sequencing of events is illustrated in the colour contour of the time-series; the beginning cycles are blue in colour and the end cycles are red in colour, with the middle cycles ranging in colour between blue and red. (A) Normalized sagittal plane T_{10}-T_{12} and S_2 angular displacement ($\theta(t)$) time series, separated by cycle. (B) Normalized angular position vs. angular velocity ($\omega(t)$) phase plots for T_{10}-T_{12} and S_2 IMUs/marker clusters. (C) Phase angle on a scale of 0° to +180° for T_{10}-T_{12} and S_2 inertial measurement units and marker clusters. (D) The CRP angle between T_{10}-T_{12} and S_2 IMUs/marker clusters ranging from −180° (indicating thorax-leading movement) to +180° (indicating pelvis-leading movement).

between 0.3 and 0.7 denote weak to moderate positive agreement, and between 0 and 0.3 is regarded as poor agreement (Cohen, 1988).

3. Results

Correlations between estimates of λ_{max} were strong when using both SS and FE data (Table 2). When using SS data, correlations between λ_{max} estimates for both T_{10}-T_{12} and S_2 marker cluster/IMU pairings were strong ($0.738 \leq ICC_{2,1}^{\lambda max,SS} \leq 0.828$); however, correlations of λ_{max} between instruments when using FE data were consistently stronger ($0.885 \leq ICC_{2,1}^{\lambda max,FE} \leq 0.919$). This trend was opposite when examining relative motion between T_{10}-T_{12} and S_2 marker cluster/IMUs ($ICC_{2,1}^{\lambda max,FE} = 0.807$; $ICC_{2,1}^{\lambda max,SS} = 0.868$).

Correlations between MARP and DP measures were strong using the FE time-series' across the entire FE cycle ($ICC_{2,1}^{MARP} = 0.963$; $ICC_{2,1}^{DP} = 0.963$). These trends were also evident when measuring MARP and DP during both solely extension- and flexion-based movements individually (Table 3).

Table 2
Mean local dynamic stability (λmax) results for individual sensors and relative (i.e., lumbar) motion. The time-series column conveys the signal that was used for calculation of λmax (FE = flexion–extension; SS = sum of squares). The last column represents the intraclass correlation coefficient of the measures between the inertial measurement unit (IMU) and Vicon systems. Errors (in brackets) depict standard deviations.

Sensor	Time-series	IMU	Vicon	$ICC_{2,1}$
T_{10}-T_{12}	FE	2.26 (0.27)	2.37 (0.28)	0.919
	SS	2.11 (0.22)	2.25 (0.26)	0.828
S_2	FE	1.88 (0.18)	1.96 (0.28)	0.885
	SS	1.80 (0.20)	1.93 (0.28)	0.738
Relative	FE	2.13 (0.24)	2.33 (0.22)	0.807
	SS	2.10 (0.19)	2.29 (0.19)	0.868

Table 3
Mean continuous relative phase results for purely flexion, extension, and flexion and extension combined. The third and sixth columns represent the intraclass correlation coefficients between inertial measurement units (IMUs) and Vicon for measuring mean absolute relative phase (MARP) and deviation phase (DP), respectively. Errors (in brackets) depict standard deviations.

	MARP			DP		
Movement	IMU	Vicon	$ICC_{2,1}$	IMU	Vicon	$ICC_{2,1}$
Flexion-Extension	−10.47 (9.12)	−10.72 (9.23)	0.963	17.40 (15.64)	15.40 (15.64)	0.963
Extension	−13.34 (12.97)	−11.61 (12.57)	0.961	16.19 (15.29)	13.94 (15.31)	0.961
Flexion	−7.96 (12.02)	−10.26 (13.14)	0.963	18.69 (16.37)	16.91 (16.51)	0.963

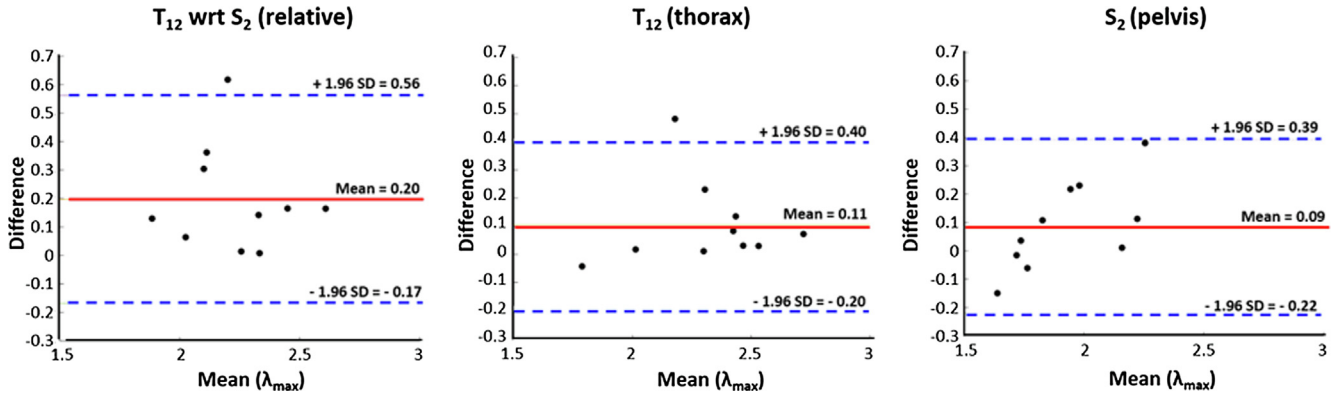

Fig. 5. Bland-Altman plots assessing level of agreement between Vicon and MetaMotionR inertial measurement units in measuring individual and relative λ_{max}.

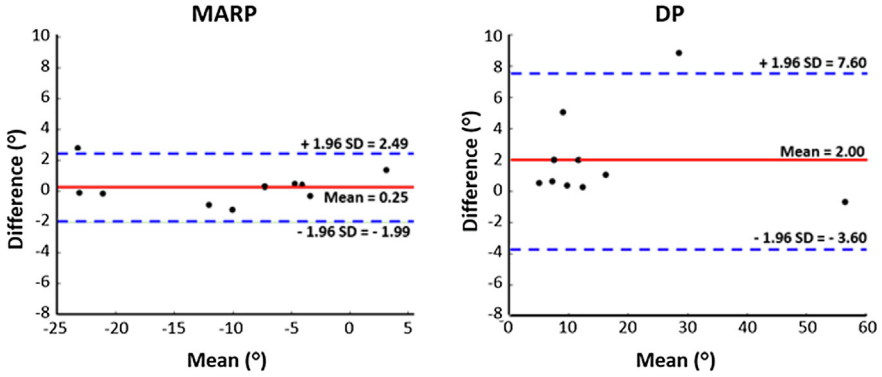

Fig. 6. Bland-Altman plots assessing level of agreement between Vicon and MetaMotionR inertial measurement units for mean absolute relative phase (MARP) and deviation phase (DP) measures in the sagittal plane.

Bland-Altman statistics revealed that all differences in measurement of λ_{max} were within 2 SDs of error, with one outlier found in all plots except for S_2 FE (no outliers were found; Fig. 5). Similarly, Bland-Altman statistics revealed that all differences in measurement of MARP and DP were within 2 SDs of error, with one outlier found in each plot (Fig. 6). There were biases of approximately 2° and 0.2 when measuring DP and λ_{max}, respectively; however, these values were within an acceptable range of SDs from existing literature (Beaudette et al., 2014; Graham et al., 2015, 2014; Granata and England, 2006; Mokhtarinia et al., 2016; Ross et al., 2015; Seay et al., 2011).

4. Discussion

Building on strong results from previous work, the purpose of the current study was to assess the accuracy and reliability of Mbientlab MetaMotionR IMUs in measuring elements of spine movement quality and control relative to conventional optical motion capture equipment. In previous work, the IMUs had strong correlations ($R > 0.99$) in the primary axis when tracking continuous 1D rotational motion (on a motorized platform), and low root-mean-square error (RMSE) $\leq 1.40°$ in all axes; however, weak-to-moderate correlations were found in one non-primary axis during all tests, and that axis was direction-dependent (Beange et al., 2018). This trend was evident in a follow-up study assessing motion tracking performance in the lumbar spine, where weak-to-moderate correlations were found in the axial twist plane during spine FE (Beange et al., 2019). Because movement in these studies was heavily dominated by primary-axis rotation, any weaker non-primary axis motion tracking would not have a large influence on the calculation of the SS for assessment of movement quality. Additionally, MARP and DP metrics are evaluated using solely FE motion, which has shown strong correlations in previous work. As such, it was hypothesized that the MetaMotionR IMUs would produce strong correlations with Vicon in measuring spine control metrics when using FE data and SS data, and that correla-

tions would be stronger when using FE data, though any differences would be negligible.

The current results demonstrate strong correlation between the MetaMotionR IMUs and Vicon in measuring λ_{max}, MARP, and DP. As predicted, stronger correlations for λ_{max} were found when using the FE time-series compared to the SS time-series for individual IMUs and marker clusters. In contrast, λ_{max} estimates for relative motion between IMUs/marker clusters demonstrate opposing results, where stronger correlations between instruments were found when using the SS rather than the FE time-series (though both were still strong). It is likely that concurrent expansion/contraction in non-primary axes during FE-based movement influenced this; that is, although each IMU was approximately oriented to capture the FE movement in a single component Euler axis, it is likely that the two coordinate systems were not perfectly aligned. Thus, there is potential to inadvertently introduce more power in the off-axis rotations for the relative motion compared to the absolute orientations for each individual sensor. This may also explain why the SS shows stronger agreement than the FE plane for relative motion; that is, absolute rotations in either direction can be nullified, yielding stronger results. As such, it is necessary in some cases to include all three component orientations in order to accurately depict the movement, as FE alone may be missing some of the overall picture. Additionally, while Bland-Altman plots revealed a bias when measuring λ_{max}, any differences were within an acceptable range (Beaudette et al., 2014; Graham et al., 2014; Granata and England, 2006).

When examining CRP features, only FE data were interpreted in accordance with the nature of the movement protocol (i.e., motion was purely FE), and to mirror clinical assessments of lumbopelvic coordination and variability (Delitto et al., 2012; Wattananon et al., 2017). In the current study, correlations for MARP and DP were strong across the entire FE cycle and during solely flexion and/or extension motion ($ICC_{2,1} > 0.96$). While Bland-Altman plots revealed instrument measurement biases for DP, any differences noted were within an acceptable range (Graham et al., 2015; Mokhtarinia et al., 2016; Seay et al., 2011). Additionally, previous work assessing thoracic-lumbar CRP in 51 healthy males reported within-group differences of up to 100° during trunk FE (Beaudette et al., 2019), confirming that within-group variability in relative PA can be large; therefore, additional analyses pertaining to within- and between-group variability are required before determining limits of what is acceptable.

The current study has several factors that likely influence motion tracking in both primary and non-primary axes. While it is assumed that rigid plate and/or IMU local coordinate systems line up with the local anatomical coordinate system (i.e., sagittal, transverse, and frontal planes of individual vertebrae) to accurately capture motion of the specified anatomical region, misalignment of the rigid plate and/or IMU can introduce potential measurement error as a result of trigonometric calculation incongruity when estimating absolute orientation (Taylor et al., 2017). An anatomical coordinate system can potentially be created for sacral and thoracic components by placing additional passive reflective markers on anatomical landmarks to transform the technical coordinate system into the anatomical coordinate system; however, this would never be feasible using IMUs, as they do not have positional information. Several attempts were made to transform local coordinate systems between Vicon and IMUs, as well as between sacral and thoracic components; however, there were no improvements to the results generated using the method described in this paper. Further refinement of local coordinate system transformations may be necessary to achieve optimal results. In the future, creating a smaller, more localized coordinate system to be tracked by Vicon (e.g., by placing 3–4 passive reflective stickers directly onto the IMU) may improve transformations between local coordinate systems of IMUs and Vicon, as well as the accuracy of vertebral body motion tracking. Additionally, exploring the effects of sensor placement accuracy and reliability in capturing movement quality features may help to achieve stronger correlations between systems. Further, due to data-acquisition limitations, individual cycles were cut based on the peak flexion angle in the sagittal plane time-series rather than global time-stamps, which has potential to introduce error in the calculation of CRP angles (i.e., improper synchronization of time-series signals from thoracic and sacral components can lead to innaccurate calculations of relative PA between the two segments). Though correlations were strong between IMUs and Vicon when calculating CRP features, future studies will parse individual cycles based on global time-stamps to ensure that accuracy is optimized. Lastly, while the current study did not explore accuracy of continuous primary- and non-primary-axis motion tracking relative to Vicon, previous studies revealed weak-to-moderate correlation in one non-primary axis for motion tracking. Conducting multi-directional movement protocols may help to identify any issues with non-primary axis motion tracking. It was also speculated that weakly correlated non-primary axes may be a result of the on-board sensor fusion process used to obtain Euler orientation from raw sensor data, with which details are unknown to the user. Therefore, future studies involving the MetaMotionR IMUs will implement custom filtering/fusion from raw sensor data to instill confidence in the processes utilized to track orientation, and to optimize these processes to achieve the strongest accuracies possible.

Overall, despite potential poor third-axis motion tracking, Mbientlab MetaMotionR IMUs are suitable for reproducing features that are representative of lumbar spine movement quality and motor control. Future studies will investigate the clinical meaning of these forms of assessment in identifying movement subgroups; in order to be regarded as clinically suitable, performance will be evaluated on both clinical and healthy populations to see if the IMUs are able to discern movement patterns between groups. Before proceeding, limits of what is acceptable when assessing performance for quantifying movement quality and control must be established.

Declaration of Competing Interest

The authors have no conflicts of interest to declare.

Acknowledgments

This study was funded by the Natural Sciences and Engineering Research Council of Canada (RGPIN-2014-05560 [Ryan Graham]; CREATE-BEST) and an Ontario Early Researcher Award (Ryan Graham).

References

Asgari, M., Sanjari, M.A., Mokhtarinia, H.R., Moeini Sedeh, S., Khalaf, K., Parnianpour, M., 2015. The effects of movement speed on kinematic variability and dynamic stability of the trunk in healthy individuals and low back pain patients. Clin. Biomech. 30 (7), 682–688.

Asgari, N., Sanjari, M.A., Esteki, A., 2017. Local dynamic stability of the spine and its coordinated lower joints during repetitive Lifting: effects of fatigue and chronic low back pain. Hum. Mov. Sci. 54, 339–346.

Ashouri, S., Abedi, M., Abdollahi, M., Dehghan Manshadi, F., Parnianpour, M., Khalaf, K., 2017. A novel approach to spinal 3-D kinematic assessment using inertial sensors: towards effective quantitative evaluation of low back pain in clinical settings. Comput. Biol. Med. 89, 144–149.

Azevedo, D.C., Ferreira, P.H., de Oliveira Santos, H., Oliveira, D.R., de Souza, J.V.L., Costa, L.O.P., 2018. Movement system impairment-based classification treatment versus general exercises for chronic low back pain: randomized controlled trial. Phys. Ther. 98 (1), 28–39.

Bauer, C.M., Rast, F.M., Ernst, M.J., Kool, J., Oetiker, S., Rissanen, S.M., Suni, J.H., Kankaanpää, M., 2015a. Concurrent validity and reliability of a novel wireless

inertial measurement system to assess trunk movement. J. Electromyogr. Kinesiol. 25 (5), 782–790.
Bauer, C.M., Rast, F.M., Ernst, M.J., Oetiker, S., Meichtry, A., Kool, J., Rissanen, S.M., Suni, J.H., Kankaanpää, M., 2015b. Pain intensity attenuates movement control of the lumbar spine in low back pain. J. Electromyogr. Kinesiol. 25 (6), 919–927.
Beange, K.H.E., Chan, A.D.C., Graham, R.B., 2019. Wearable sensor performance for motion tracking of the lumbar spine. In: The 42nd Canadian Medical and Biological Engineering Conference.
Beange, K.H.E., Chan, A.D.C., Graham, R.B., 2018. Evaluation of wearable IMU performance for orientation estimation and motion tracking. In: IEEE Int. Symp. Med. Meas. Appl.
Beaudette, S.M., Graham, R.B., Brown, S.H.M., 2014. The effect of unstable loading versus unstable support conditions on spine rotational stiffness and spine stability during repetitive lifting. J. Biomech. 47 (2), 491–496.
Beaudette, S.M., Zwambag, D.P., Graham, R.B., Brown, S.H.M., 2019. Discriminating spatiotemporal movement strategies during spine flexion-extension in healthy individuals. Spine J. 19 (7), 1264–1275.
Biely, S.A., Silfies, S.P., Smith, S.S., Hicks, G.E., 2014. Clinical observation of standing trunk movements: what do the aberrant movement patterns tell us?. J. Orthop. Sports Phys. Ther. 44 (4), 262–272.
Bolink, S.A.A.N., Naisas, H., Senden, R., Essers, H., Heyligers, I.C., Meijer, K., Grimm, B., 2016. Validity of an inertial measurement unit to assess pelvic orientation angles during gait, sit – stand transfers and step-up transfers: comparison with an optoelectronic motion capture system. Med. Eng. Phys. 38 (3), 225–231.
Bosch Sensortec, 2015. Integration Guideline for BSXlite Library.
Bruijn, S.M., van Dieën, J.H., Meijer, O.G., Beek, P.J., 2009a. Statistical precision and sensitivity of measures of dynamic gait stability. J. Neurosci. Methods 178 (2), 327–333.
Bruijn, S.M., van Dieën, J.H., Meijer, O.G., Beek, P.J., 2009b. Is slow walking more stable?. J. Biomech. 42 (10), 1506–1512.
Cohen, J., 1988. Statistical Power Analysis for the Behavioural Sciences. Lawrence Erlbaum Associates, Hillsdale, NJ.
Cuesta-Vargas, A.I., Galán-Mercant, A., Williams, J.M., 2010. The use of inertial sensors system for human motion analysis. Phys. Ther. Rev. 15 (6), 462–473.
Delitto, A., George, S.Z., Dillen, L. Van, Whitman, J.M., Sowa, G.A., 2012. Low back pain: clinical practice guidelines linked to the international classification of functioning, disability, and health from the orthopaedic section of the American Physical Therapy Association. J. Orthop. Sport. Phys. Ther. 42 (4), A1–A57.
Dillingham, T.R., 1995. Evaluation and management of low back pain: an overview. Spine: State Art Rev. 9 (3), 559–574.
Fritz, J.M., Cleland, J.A., Childs, J.D., 2007. Subgrouping patients with low back pain: evolution of a classification approach to physical therapy. J. Orthop. Sports Phys. Ther. 37 (6), 290–302.
Graham, R.B., Brown, S.H.M., 2012. A direct comparison of spine rotational stiffness and dynamic spine stability during repetitive lifting tasks. J. Biomech. 45 (9), 1593–1600.
Graham, R.B., Oikawa, L.Y., Ross, G.B., 2014. Comparing the local dynamic stability of trunk movements between varsity athletes with and without non-specific low back pain. J. Biomech. 47 (6), 1459–1464.
Graham, R.B., Sadler, E.M., Stevenson, J.M., 2012a. Local dynamic stability of trunk movements during the repetitive lifting of loads. Hum. Mov. Sci. 31 (3), 592–603.
Graham, R.B., Sheppard, P.S., Almosnino, S., Stevenson, J.M., 2012b. Dynamic spinal stability and kinematic variability across automotive manufacturing work shifts and days. Int. J. Ind. Ergon. 42 (5), 428–434.
Graham, R.B., Smallman, C.L.W., Miller, R.H., Stevenson, J.M., 2015. A dynamical systems analysis of assisted and unassisted anterior and posterior hand-held load carriage. Ergonomics 58 (3), 480–491.
Granata, K.P., England, S.A., 2006. Stability of dynamic trunk movement. Spine (Phila. Pa. 1976) 31 (10), E271–E276.
Hamill, J., Palmer, C., Van Emmerik, R.E.A., 2012. Coordinative variability and overuse injury. Sports Med. Arthrosc. Rehabil. Ther. Technol. 4 (1), 1–9.
Hemming, R., Sheeran, L., van Deursen, R., Sparkes, V., 2018. Non-specific chronic low back pain: differences in spinal kinematics in subgroups during functional tasks. Eur. Spine J. 27 (1), 163–170.
Hicks, G.E., Fritz, J.M., Delitto, A., Mishock, J., 2003. Interrater reliability of clinical examination measures for identification of lumbar segmental instability. Arch. Phys. Med. Rehabil. 84 (12), 1858–1864.
Hodges, P.W., Van Dillen, L.R., McGill, S., Brumagne, S., Hides, J.A., Moseley, G.L., 2013. Chapter 21: Integrated clinical approach to motor control interventions in low back and pelvic pain, Spinal Control: The Rehabilitation of Back Pain: State of the art and science. Elsevier Ltd..
Howarth, S.J., Graham, R.B., 2015. Sensor positioning and experimental constraints influence estimates of local dynamic stability during repetitive spine movements. J. Biomech. 48 (6), 1219–1223.
Hoy, D., Brooks, P., Blyth, F., Buchbinder, R., 2010. The epidemiology of low back pain. Best Pract. Res. Clin. Rheumatol. 24 (6), 769–781.
Kim, S., Nussbaum, M.A., 2013. Performance evaluation of a wearable inertial motion capture system for capturing physical exposures during manual material handling tasks. Ergonomics 56 (2), 314–326.
Laird, R.A., Kent, P., Keating, J.L., 2016. How consistent are lordosis, range of movement and lumbo-pelvic rhythm in people with and without back pain? BMC Musculoskelet. Disord. 17, 403.
Lamb, P.F., Stöckl, M., 2014. On the use of continuous relative phase: review of current approaches and outline for a new standard. Clin. Biomech. 29 (5), 484–493.
Maher, C., Underwood, M., Buchbinder, R., 2017. Non-specific low back pain. Lancet 389 (10070), 736–747.
Mokhtarinia, H.R., Sanjari, M.A., Chehrehrazi, M., Kahrizi, S., Parnianpour, M., 2016. Trunk coordination in healthy and chronic nonspecific low back pain subjects during repetitive flexion-extension tasks: effects of movement asymmetry, velocity and load. Hum. Mov. Sci. 45, 182–192.
O'Sullivan, P., 2005. Diagnosis and classification of chronic low back pain disorders: Maladaptive movement and motor control impairments as underlying mechanism. Man. Ther. 10 (4), 242–255.
Peters, B.T., Haddad, J.M., Heiderscheit, B.C., Van Emmerik, R.E.A., Hamill, J., 2003. Limitations in the use and interpretation of continuous relative phase. J. Biomech. 36 (2), 271–274.
Rosenstein, M.T., Collins, J.J., De Luca, C.J., 1993. A practical method for calculating largest Lyapunov exponents from small data sets. Phys. D Nonlinear Phenom. 65 (1–2), 117–134.
Ross, G.B., Mavor, M.P., Brown, S.H.M., Graham, R.B., 2015. The effects of experimentally induced low back pain on spine rotational stiffness and local dynamic stability. Ann. Biomed. Eng. 43 (9), 2120–2130.
Seay, J.F., Van Emmerik, R.E.A., Hamill, J., 2011. Low back pain status affects pelvis-trunk coordination and variability during walking and running. Clin. Biomech. 26 (6), 572–578.
Silfies, S.P., Bhattacharya, A., Biely, S., Smith, S.S., Giszter, S., 2009. Trunk control during standing reach: a dynamical system analysis of movement strategies in patients with mechanical low back pain. Gait Posture 29 (3), 370–376.
Spinelli, B.A., Wattananon, P., Silfies, S., Talaty, M., Ebaugh, D., 2015. Using kinematics and a dynamical systems approach to enhance understanding of clinically observed aberrant movement patterns. Man. Ther. 20 (1), 221–226.
Stanton, T.R., Fritz, J.M., Hancock, M.J., Latimer, J., Maher, C.G., Wand, B.M., Parent, E. C., 2011. Evaluation of a treatment-based classification algorithm for low back pain: a cross-sectional study. Phys. Ther. 91 (4), 496–509.
Stergiou, N., Jensen, J.L., Bates, B.T., Scholten, S.D., Tzetzis, G., 2001. A dynamical systems investigation of lower extremity coordination during running over obstacles. Clin. Biomech. 16 (3), 213–221.
Taylor, L., Miller, E., Kaufman, K.R., 2017. Static and dynamic validation of inertial measurement units. Gait and Posture 57 (September), 80–84.
van Dieën, J.H., Reeves, N.P., Kawchuk, G., Dillen, L. Van, Hodges, P.W., 2018a. Analysis of motor control in low-back pain patients, a key to personalized care? J. Orthop. Sport. Phys. Ther. 49 (6), 380–388.
van Dieën, J.H., Reeves, N.P., Kawchuk, G., van Dillen, L., Hodges, P.W., 2018b. Motor control changes in low-back pain: divergence in presentations and mechanisms. J. Orthop. Sport. Phys. Ther. 49 (6), 370–379.
van Dieën, J.H., van Drunen, P., Happee, R., 2018c. Sensory contributions to stabilization of trunk posture in the sagittal plane. J. Biomech. 70, 219–227.
Vos, T. et al., 2016. Global, regional, and national incidence, prevalence, and years lived with disability for 310 diseases and injuries, 1990–2015: a systematic analysis for the Global Burden of Disease Study 2015. Lancet 388 (10053), 1545–1602.
Waddell, G., 2004. The Back Pain Revolution. Elsevier Health Sciences.
Wattananon, P., Ebaugh, D., Biely, S., Smith, S.S., Hicks, G.E., Silfies, S.P., 2017. Kinematic characterization of clinically observed aberrant movement patterns in patients with non-specific low back pain: a cross-sectional study. BMC Musculoskelet. Disord. 18 (1), 455.
Whelan, D., Reilly, M.O., Huang, B., Giggins, O., Kechadi, T., 2016. Leveraging IMU Data for Accurate Exercise Performance Classification and Musculoskeletal Injury Risk Screening. In: IEEE Eng in Med and Biol Soc.
Winter, D.A., 2010. Biomechanics and Motor Control of Human Movement. John Wiley & Sons Inc, Hoboken, New Jersey.